Zeolite Waste Characterization and Use as Low-Cost, Ecofriendly, and Sustainable Material for Malachite Green and Methylene Blue Dyes Removal: Box-Behnken Design, Kinetics, and Thermodynamics

Ali Imessaoudene, Sabrina Cheikh, Jean-Claude Bollinger, Lazhar Belkhiri, Ammar Tiri, Abdelkrim Bouzaza, Atef El Jery, Aymen Assadi, Abdeltif Amrane, Lotfi Mouni

applied sciences

MDPI

Article

Zeolite Waste Characterization and Use as Low-Cost, Ecofriendly, and Sustainable Material for Malachite Green and Methylene Blue Dyes Removal: Box–Behnken Design, Kinetics, and Thermodynamics

Ali Imessaoudene [1,2], Sabrina Cheikh [1,2], Jean-Claude Bollinger [3], Lazhar Belkhiri [4], Ammar Tiri [4], Abdelkrim Bouzaza [5], Atef El Jery [6], Aymen Assadi [5], Abdeltif Amrane [5,*] and Lotfi Mouni [1,*]

1 Laboratoire de Gestion et Valorisation des Ressources Naturelles et Assurance Qualité, Faculté SNVST, Université de Bouira, Bouira 10000, Algeria; a.imessaoudene@univ-bouira.dz (A.I.); chikhsabrina@yahoo.fr (S.C.)
2 Département de Génie des Procédés, Faculté de Technologie, Université de Bejaia, Bejaia 06000, Algeria
3 Laboratoire E2Lim (Eau Environnement Limoges), Université de Limoges, 123 Avenue Albert Thomas, 87060 Limoges, France; jean-claude.bollinger@unilim.fr
4 Département d'Hydraulique, Université de Batna, Batna 05000, Algeria; belkhiri.la@gmail.com (L.B.); tiriammar@yahoo.fr (A.T.)
5 Univ Rennes, Ecole Nationale Supérieure de Chimie de Rennes, CNRS, ISCR—UMR 6226, 35000 Rennes, France; abdelkrim.bouzaza@ensc-rennes.fr (A.B.); aymen.assadi@ensc-rennes.fr (A.A.)
6 Department of Chemical Engineering, College of Engineering, King Khalid University, Abha 61411, Saudi Arabia; ajery@kku.edu.sa
* Correspondence: abdeltif.amrane@univ-rennes1.fr (A.A.); lotfimouni@gmail.com (L.M.)

check for updates

Citation: Imessaoudene, A.; Cheikh, S.; Bollinger, J.-C.; Belkhiri, L.; Tiri, A.; Bouzaza, A.; El Jery, A.; Assadi, A.; Amrane, A.; Mouni, L. Zeolite Waste Characterization and Use as Low-Cost, Ecofriendly, and Sustainable Material for Malachite Green and Methylene Blue Dyes Removal: Box–Behnken Design, Kinetics, and Thermodynamics. *Appl. Sci.* **2022**, *12*, 7587. https://doi.org/10.3390/app12157587

Academic Editor: Rajender S. Varma

Received: 6 June 2022
Accepted: 24 July 2022
Published: 28 July 2022

Publisher's Note: MDPI stays neutral with regard to jurisdictional claims in published maps and institutional affiliations.

Abstract: This study investigated the potential of 4A zeolite, named4AZW in this work, generated by natural gas dehydration units as solid waste after several treatment cycles, as a low-cost adsorbent to separately remove two cationic dyes, methylene blue (MB) and malachite green (MG), from an aqueous solution within a batch process. The adsorbent material was characterized by N_2gas adsorption–desorption, X-ray fluorescence spectrometry, X-ray diffraction, FT-IR spectroscopy, and the determination of its cation exchange capacity and point of zero charge. The influence of key operating parameters, such as the pH, adsorbent dosage, ionic strength, contact time, initial dye concentration, and temperature, was investigated. Three independent variables acting on MB adsorption performance were selected from the Box–Behnken design (BBD) and for process modeling and optimization. An analysis of variance (ANOVA), an F-test, and p-values were used to analyze the main and interaction effects. The experimental data were satisfyingly fitted with quadratic regression with adjusted R^2= 0.9961. The pseudo-second-order kinetic model described the adsorption of the dyes on 4AZW. The equilibrium data were well-fitted by the Langmuir model for each adsorption system (MB-4AZW and MG-4AZW) with maximum adsorption capacity (q_{max}) values of 9.95 and 45.64 mg/g, respectively, at 25 °C. Thermodynamics studies showed that both adsorption systems are spontaneous and endothermic.

Keywords: 4A zeolite reuse; dye removal; adsorption kinetics; isotherms; response surface methodology

1. Introduction

Fossil fuels have always been the primary source of the global energy supply. Algeria has an important energy potential: It holds the tenth largest gas reserve in the world and the third largest oil reserves in Africa [1]. Among all fossil fuel energy sources, natural gas (NG) is the cleanest and is a safe source when transported, stored, and used [2]. The chemical composition of the crude NG found in oil and gas reservoirs is composed of methane (as a major component), and in smaller quantities, ethane, propane, and butane, among other gaseous hydrocarbons. It also contains undesirable compounds such as water

vapor, carbon dioxide, nitrogen, and hydrogen sulfide [3,4]. In industrial use, natural gas is subjected to different cleaning processes to meet product quality standards. Two main standards can be distinguished: Liquid natural gas (LNG) and pipeline gas [5]. The water vapor contained in NG must be removed from the gas stream for the following reasons: Reducing the heating value of the produced gas, condensation of the water in the pipelines, and the risk of corrosion [2].

Extensive literature is available on common gas dehydration systems including glycol absorption, zeolite adsorption, and refrigeration-based systems [6]. Among these processes, adsorption on zeolite, especially the Temperature Swing Adsorption (TSA) system, is the most frequently used industrially for technical and energetic considerations [7]. The simplest configuration for the application of a TSA system to obtain a continuous flow of produced gas is the fixed double-bed system, with one operating in adsorption mode and the second in desorption mode (regeneration) [5]. Due to the higher capacity of water adsorption and selectivity, as well as its regeneration potential for several cycles of adsorption, the 4A zeolite adsorbent is widely used for the fine drying of NG in the TSA system [5,7].

Zeolites [8] are crystalline microporous aluminosilicates with a three-dimensional framework structure bearing AlO_4 and SiO_4 tetrahedra. These are linked to each other by sharing all of the oxygen to form interconnected cages and channels [9] with the characteristics of high ion exchange capacity and excellent selectivity (size, charge, and shape) and porosity on the surface [10]. Zeolites present a high potential for the purification of gases, especially those containing moisture [11]. 4A zeolite belongs to the LTA-type, with a pore size of 0.4 nm and a Si/Al ratio of approximately 1. This low Si/Al ratio, owing to the high aluminum content, makes the material highly hydrophilic [12]. The dehydration unit in the gas plant TFT of the Sonatrach company in Algeria generates important amounts of 4A zeolites after using the material in several adsorption and regeneration cycles, which reduces its adsorptive capacity with respect to the desired product quality during the dehydration operation. Under such a situation, the adsorbent is treated as solid waste to be disposed of in the technical landfill center near the plant site. The reuse of this adsorbent in wastewater treatment can be a possible way to valorize it by increasing its lifetime before it is considered waste. Several studies have applied natural and synthetic zeolites [13–18], as well as other eco-friendly materials [19], in wastewater treatment.

In the present paper, batch experiments were carried out to separately remove methylene blue (MB) or malachite green (MG), two very popular and toxic cationic dyes [20,21], by the adsorption technique using 4A zeolite solid waste from the gas dehydration unit of TFT plant (Sonatrach company). This adsorbent material is named '4A zeolite waste' (4AZW) here. The characterization of the 4AZW sample was performed by BET surface area analysis, X-ray diffraction, and FT-IR analysis. The influence of temperature, pH, amount of adsorbent, contact time, and initial MB or MG concentrations on the removal rate of those dyes were studied under shaken conditions. Different classical kinetic models were used to interpret the adsorption of each dye on 4AZW. Experimental equilibrium data were fitted with Freundlich and Langmuir isotherm equations to determine the best-fitting model. Additionally, in this work, it has been established that pH, the initial concentration, and the amount of adsorbent interacted and ultimately affected MB removal efficiency by the response surface methodology (RSM). This approach is a statistical application on the basis of fitting empirical models to a set of data obtained from several experiments: It is considered one of the most multivariate techniques used in process optimization [22,23]. By collectively optimizing all the affecting parameters, RSM can eliminate the limitations of single factor-at-a-time experiments [24,25]. This global investigation allowed for the study of new kinds of Zeolites.

This study on the investigation of the potential of 4AZW for the removal of two basic cationic dyes, MB and MG, from aqueous solutions under batch experimental conditions shows that wastewater treatment with this kind of zeolite constitutes an economical and

efficient way to eliminate aqueous pollutants, which clearly meets the main aims of the UN Sustainable Development Goals (UN SDGs).

2. Materials and Methods

2.1. Materials

The 4AZW used in this study was obtained from the gas dehydration unit of the TFT plant (Sonatrach company, Hydra, Algeria). This material was received as a binder-containing zeolite in the form of cylindrical pellets. After crushing, 100 g of the raw sample with a particle size lower than 100 µm was dried at 110 °C for two hours and then dispersed in 1 L of deionized water and mixed for 24 h to eliminate all water-soluble impurities. After solid–liquid separation by filtration under a vacuum with Whatman® paper filter grade 40 (particle retention 8 µm), the obtained residue was calcined at 450 °C for 2 h to eliminate all the organic compounds possibly retained during its initial use in the dehydration of the gas and finally kept in a desiccator until tested.

Two cationic dyes were selected for this study: Methylene blue (MB) and Malachite green (MG), obtained from Biochem Chemopharma (Cosne-Cours-sur-Loire, France). The maximum absorbance wavelengths of MB (664 nm) and MG (620 nm) were determined with a double beam UV–vis spectrometer (Specord 200 plus).

2.2. Characterization of 4AZW

The physicochemical properties of the solid material were determined using standard analytical techniques. To obtain the specific surface area and pore structure of the material, the Nitrogen adsorption–desorption isotherms at 77 K were measured with an automated gas adsorption analyzer ASAP2000 (Micromeritics, Norcross, GA, USA) with ±5% accuracy. The total contents of chemical components were determined by X-ray fluorescence spectrometry (XRF) using a Philips PW-2400 X-ray spectrophotometer with Rh and Au excitation tubes. The X-ray diffraction (XRD) analysis of the samples was carried out via a powder X-ray diffractometer (Bruker AXS) in the angular range of 2–60° in steps of2θ with a scan rate of 0.025°/s. For Fourier-Transform Infrared spectroscopy (FT-IR, Bruker ALPHA), the spectrum was recorded in the 400–4000 cm^{-1} range.

The pH of 4AZW was measured as follows: A 1:2 (w:v) 4AZW: distilled water suspension was shaken for 24 h at 30 °C, then filtered, and the pH of the filtrate was determined by a pH-meter [26]. The cation exchange capacity (CEC) of 4AZW was determined by the $BaCl_2$-triethanolamine procedure [27]. To determine the point of zero charge (pHPZC) of the material, the 'drift method' was applied [28]: 0.2 g of adsorbent was added to 40 mL of the 0.1 mol/L NaCl solution at different initial pH values (pH_i) in the range of 3 to 12, and agitated for 24h at room temperature; the final pH (pH_f) values of solutions were then measured, and ΔpH is plotted vs. pH_i.

2.3. Adsorption Methodology

Batch adsorption experiments on the 4AZW adsorbent were conducted with either MB or MG aqueous solutions. A stock solution of MB or MG (1000 mg/L) was prepared by dissolving an accurately weighed quantity (1.0 g) of solid dye in 1 L of deionized water; the solutions for adsorption tests were diluted from the stock solution to the desired concentration.

One hundred milliliters of the dye solution at various concentrations were placed in 250 mL PE flasks with 0.1 g of the adsorbent and shaken (Labwit ZWY-304) at a speed of 200 rpm. The experiments were carried out at different pH (from 3 to 12) and temperature (from 25 to 50 °C) values. The initial pH of the solution was adjusted to the desired value by using either HCl or NaOH solutions (0.1 mol/L). Kinetics of adsorption was determined by analyzing the dye uptake at different time intervals. From the kinetic experiments, a time contact equal to 110 min was fixed for all following isotherm experiments in order to reach a steady-state or pseudo-equilibrium. Solid and solution were separated using a 0.22 µm cellulose acetate membrane filter, then the concentration of MB or MG in the

supernatant was determined by a double-beam UV/vis spectrophotometer (SPECORD 200 plus). Kinetics of adsorption was determined by analyzing the dye uptake at different time intervals.

Each experiment was carried out in triplicate and all calculations were conducted with their average values; the maximum difference between the three values was less than 3% of the mean. The adsorbed amount of MB or MG at equilibrium was calculated by the straightforward equation:

$$q_e = \frac{(C_0 - C_e).V}{m} \quad (1)$$

where q_e (mg/g) is the equilibrium adsorption capacity of dye adsorbed per gram of 4AZW, C_0 and C_e are the initial and equilibrium concentrations (mg/L) of MB or MG, respectively, V (L) is the volume of the dye solution, and m (g) is the weight of 4AZW. A linear calibration curve was prepared with MB (R^2 = 0.997) and GM (R^2 = 0.999) for UV/vis quantification.

The adsorption yield (% removal from aqueous solution) of the dye is calculated as:

$$\text{Yield } (\%) = \frac{(C_0 - C_e).100}{C_0} \quad (2)$$

2.4. Experimental Design

To better understand the effect of important parameters such as pH, the initial concentration, and the amount of adsorbent, a Box–Behnken design was applied to the removal of MB, here selected as a dye model. In order to obtain the most important independent and influential variables with the minimum number of runs, the response surface methodology (RSM) proceeds by a two-in-one technique, i.e., both mathematical and statistical techniques are used together to obtain a relationship between a response, here defined by the yield removal (Yield (%)) as the dependent variable, and a number of independent variables defined by $X_1, X_2, \ldots, X_n$. Usually, RSM is combined with factorial design methods such as the Box–Behnken design (BBD), i.e., a second-order multivariate design based on a three-level incomplete factorial design with no axial points [29].

In our case, fifteen experiments were performed with three replicates at the center point to estimate the pure error. Minitab® 17 software was used to apply the BBD model. Experimental data were fitted to a quadratic model using a second-order polynomial model as follows:

$$\text{Yield}(\%) = \beta_0 + \sum_{i=1}^{n} \beta_i.X_i + \sum_{i=1}^{n} \beta_{ii}.X_i^2 + \sum_{i=1}^{n-1} \sum_{j=i+1}^{n} \beta_{ij}.X_i.X_j + \varepsilon \quad (3)$$

where n, β_0, β_i, X_i and X_j, β_{ii}, β_{ij} and ε represent the number of variables, a constant term, the coefficients of the linear parameters, the variables, the coefficients of the quadratic parameters, the coefficients of the interaction parameters, and the residual associated with the experiments, respectively. A total of 15 experiments were needed to estimate the removal of MB on 4AZW.

The predicted values for the yield removal of MB were then obtained by applying the quadratic model. The accuracy and fitness of the model were evaluated by an analysis of variance (ANOVA): Various descriptive statistic parameters were used such as the *p*-value, an F-test, degrees of freedom (df), the determination coefficient (R^2), and the adjusted determination coefficient (R^2adj) [30,31]. Moreover, 3D-surface plots also allowed to describe the effect on the desired response of interaction between two-by-two factors [32].

3. Results and Discussion

3.1. Characterization of Material

The physicochemical properties of the 4AZW sample are presented in Table 1. XRF measurement showed that the main chemical components of the 4AZW are SiO, Al_2O_3, Na_2O, Fe_2O_3, CaO and K_2O. The XRD pattern of our sample (Figure 1) corresponds well

with the crystalline peaks of pure 4A zeolite. The diffraction peaks at 7.18°, 10.17°, 12.46°, 16.11°, 21.66°, 23.99°, 26.10°, 27.11°, 29.94°, 32.54°, and 34.17° are associated with (200), (220), (222), (420), (442), (622), (640), (642), (820), (840), and (664) crystal planes of 4A zeolite, respectively [10,33], indicating that the 4AZW has not undergone a serious loss in its crystalline structure.

Table 1. Physicochemical properties of 4AZW.

	Typical Parameters	Value
Chemical composition	SiO_2 (%)	55.39 ± 0.88
	Al_2O_3 (%)	27.18 ± 0.64
	Na_2O (%)	4.49 ± 0.52
	K_2O (%)	1.03 ± 0.12
	CaO (%)	3.34 ± 0.41
	P_2O_5(%)	0.79 ± 0.08
	Fe_2O_3 (%)	4.47 ± 0.49
	TiO_2 (%)	0.32 ± 0.04
	MgO (%)	2.99 ± 0.31
	S_{BET} (m^2/g)	35.5 ± 0.3
CEC (meq/100 g)		120 ± 6
pH (1:2 w:v slurry)		11 ± 0.1
pH_{PZC}		10.5 ± 0.1

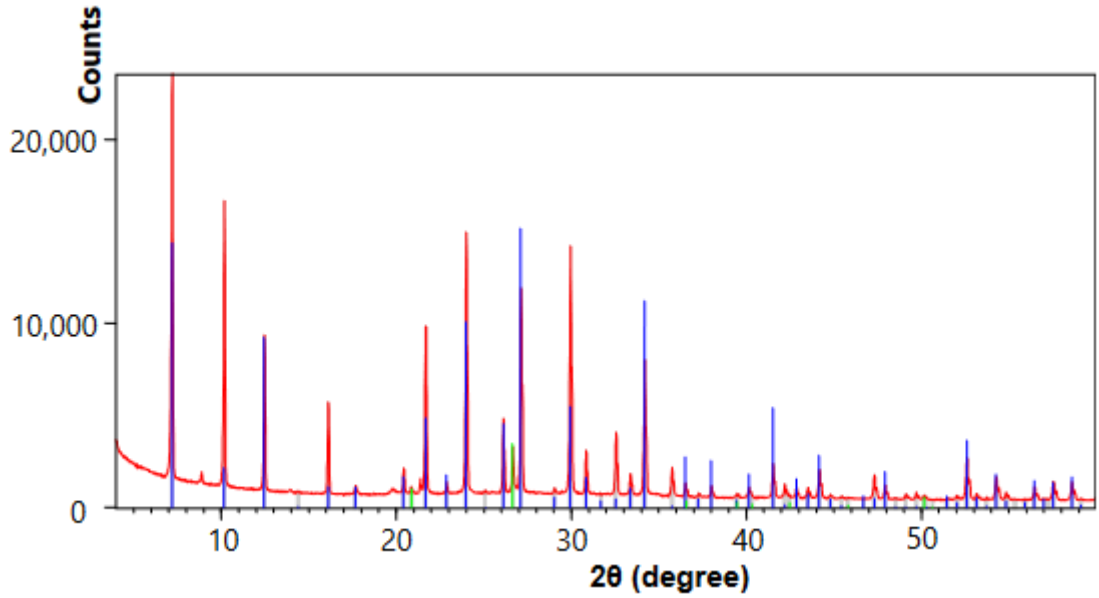

Figure 1. XRD pattern of 4AZW.

As shown in Table 1, the cation exchange capacity is 120 meq/100 g. The synthesized material exhibits strong basicity (pH = 11 for the suspension slurry) suggesting the presence of negative charges on the solid surface in an aqueous solution; this is also confirmed by the value of pH_{PZC} = 10.5 (see below). The BET/N_2 specific surface area was 35.5 m^2/g.

From FT-IR spectroscopy (Figure 2), the broad band at 3441 cm^{-1} and the sharp absorption bond at 1660 cm^{-1} correspond to the stretching and bending vibration bands of H-O-H derived from H_2O present in 4AZW [34]. In addition, there are four distinct absorption bands at 994, 787, 684, and 464 cm^{-1}, which are assigned to the asymmetric stretching vibrations of bridge bonds T-O-(T) where (T=Si or Al), symmetric stretching vibrations of bridge bonds Si-O-Si, symmetric stretching vibrations of bridge bonds Si-O-Al, and the bending vibrations O-Si-O, respectively [35].

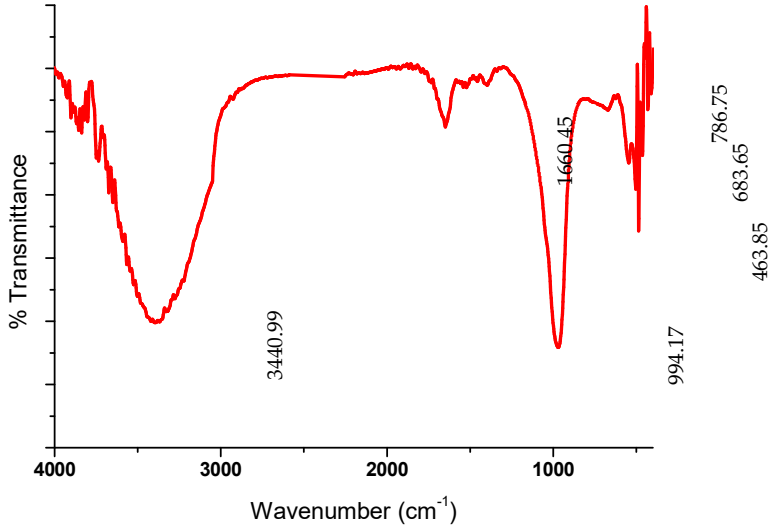

Figure 2. FT-IR spectra of 4AZW.

3.2. Effect of Initial Dye Concentration

Contact time data allow us to select the optimum shaking time to achieve a steady-state of pseudo-equilibrium of the process. The corresponding data for the removal of MB and MG are shown in Figure 3, hence the plateau becomes evident.

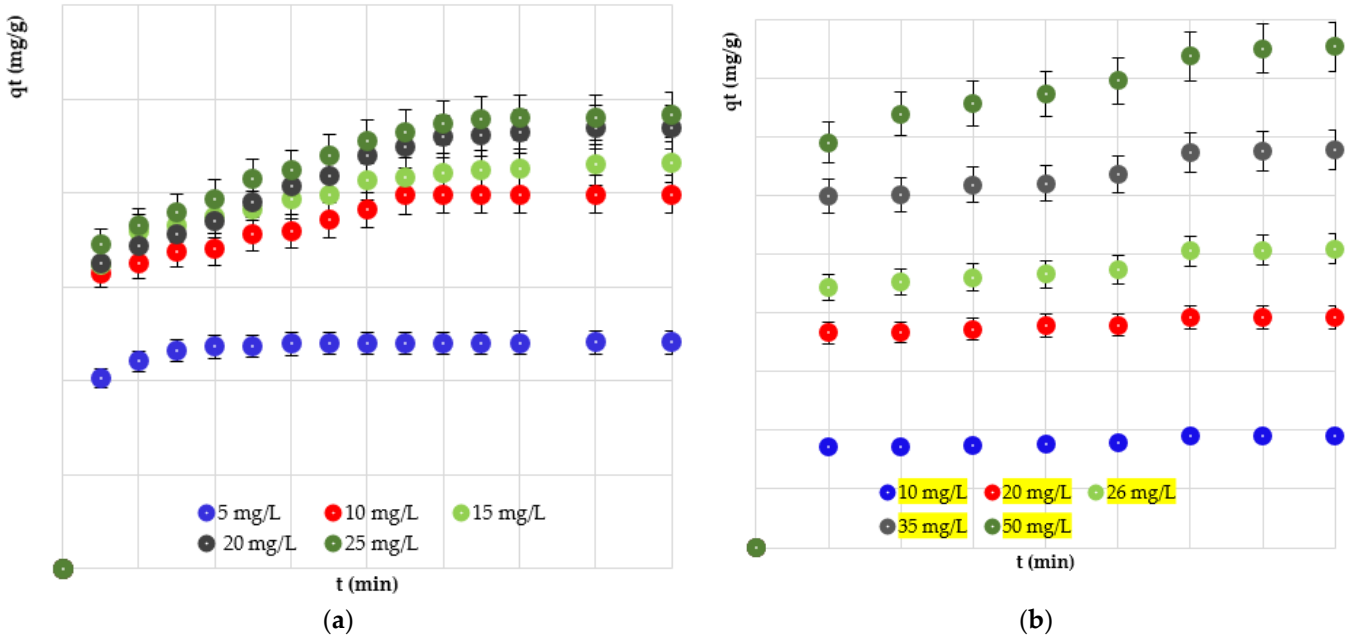

Figure 3. Effect of contact time and initial concentration of dyes: (**a**) MB; (**b**) MG on the adsorption capacity of 4AZW (S/L = 1 g/L, T = 25 ± 1 °C and unadjusted pH).

The qe values of both MB and MG sharply increased from 10 min to 50 min and balanced beyond 70 min contact time. This can be related to the number of initially vacant surface sites at the beginning. Over time, repulsive forces between the cationic dye molecules adsorbed on the surface of 4AZW and the solution phase make the remaining vacant surface sites more difficult to be occupied; thus, the adsorption slows down and finally levels off. As can be considered obvious, increasing the initial concentration will provide more driving force to overcome the mass transfer resistance between the solid and liquid phases, then the qe values increase [36].

3.3. Effect of theAdsorbent Dose

The effect of the mass of adsorbent (0.25 to 3.0 g/L) on the adsorption capacity and the percentage of dye removal showed (Figure 4) that the removal of each dye increased when the adsorbent amount increased, which could be attributed to the greater availability of adsorption sites; after reaching a plateau, one can observe the steady-state of the (pseudo) equilibrium, likely because of the saturation of the available adsorption sites as already reported in several papers [37,38]. For the following investigations, equilibrium was attained with a selected adsorbent dosage of 1 g/L.

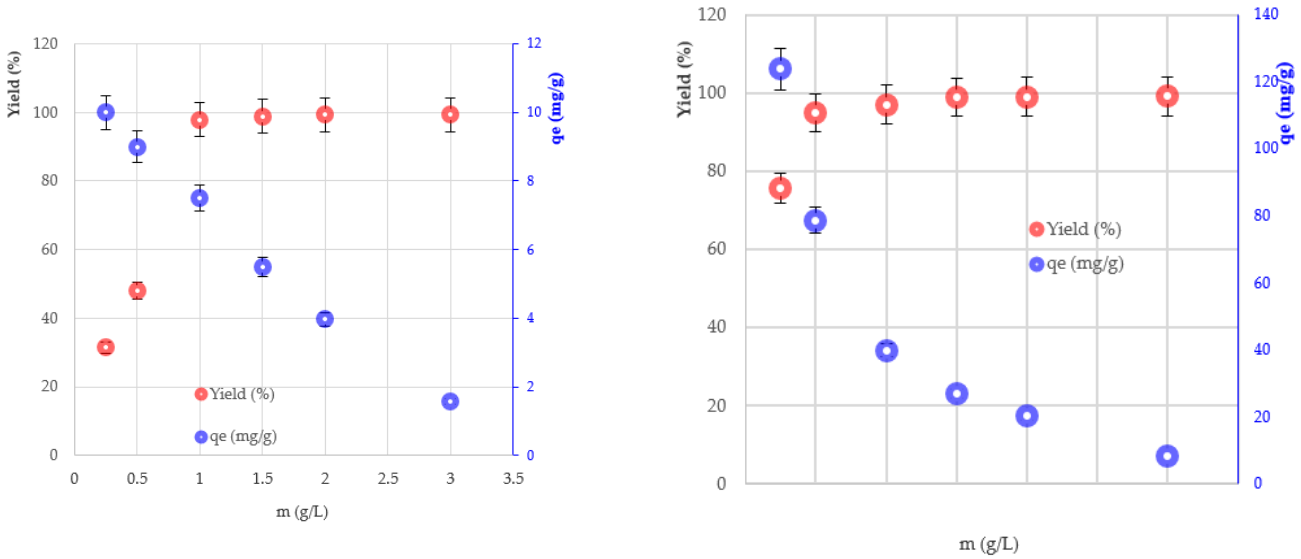

(**a**) (**b**)

Figure 4. Effect of adsorbent dosage on the percentage of removal and amount of dyes adsorbed on 4AZW: (**a**) MB; (**b**) MG (C0(MB) = 8 mg/L, C0(MG) = 41 mg/L, contact time 70 min, T = 25 ± 1 °C and unadjusted pH).

On the other hand, the increase in the adsorbent mass led to a decrease in the amount of dye uptake per gram of adsorbent (q_e). This drop in adsorption capacity is likely due to sites remaining unsaturated during adsorption [39,40] and particle aggregation [41].

3.4. Effect of Ionic Strength

As can be observed from Figure 5, the co-existence of sodium cations and dye molecules in the solution decreases the adsorption yield. Furthermore, the increase in the ionic strength is unfavorable to the adsorption efficiency. Because the ionic strength of the solution controls either electrostatic or non-electrostatic interactions between the adsorbate and the adsorbent surface [42], the electrostatic attraction mechanism for our cationic dyes can be suppressed with the addition of Na^+ ions at a high concentration, due to the competition for the active sites on the adsorbent surface, leading to electrostatic repulsion [43].

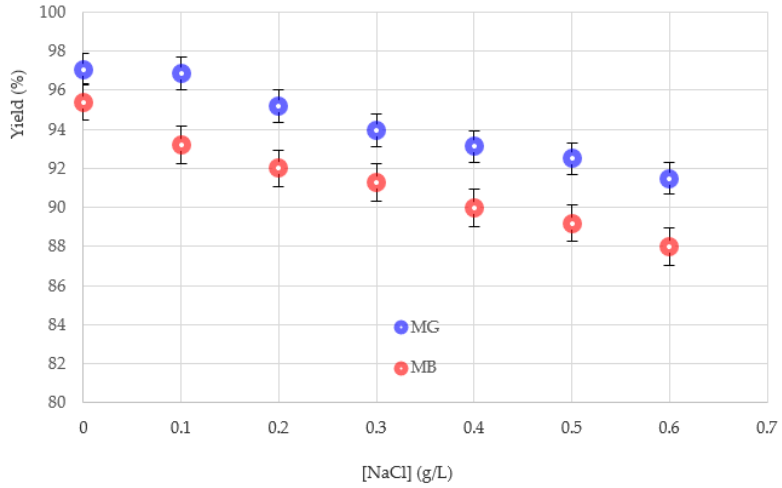

Figure 5. Effect of NaCl concentration on the adsorption percentage of MB and MG (C_0(MB) = 8 mg/L, C_0(MG) = 41 mg/L, S/L = 1 g/L, contact time 70 min, T = 25 ± 1 °C and unadjusted pH).

3.5. Effect of Solution pH

The pHpzc value of 4AZW is 10.5 (Figure 6). Then, at pH < pHpzc, the surface of the adsorbent is predominantly positive; while when the solution pH > pHpzc, the adsorbent surface is predominantly negative [44]. The effect of the initial solution's pH (in the range of 3 to 12) on the removal of each dye, at initial concentrations of MB and MG of 11.5 mg/L and 45 mg/L, respectively, at 25 °C, is shown in Figure 7.

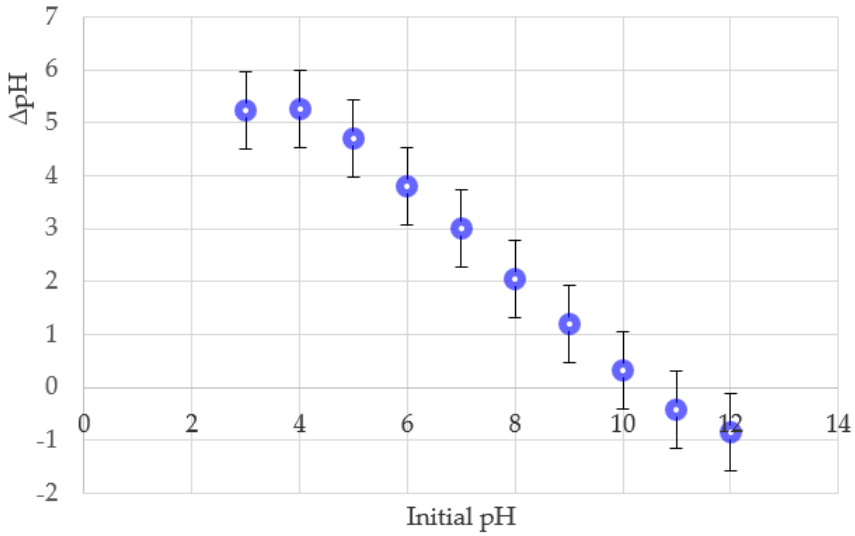

Figure 6. The plot of ΔpH vs. initial pH for the determination of 4AZW's point of zero charge.

Generally, for a cationic dye, at a lower pH, the percentage of dye removal will decrease, but it will increase at higher pH values [45]. Although methylene blue has no determinable pKa between pH 0 and 14, it is in the form MB^+ in this aqueous pH range, but several species can be formed according to the redox status of the solution [46]; for malachite green, however, pKa = 6.90 [47]. Then, for MB or MG cations, the protonated form is the predominant species in solutions at pH < pKa, and above this pH value, the dye becomes ever more de-protonated.

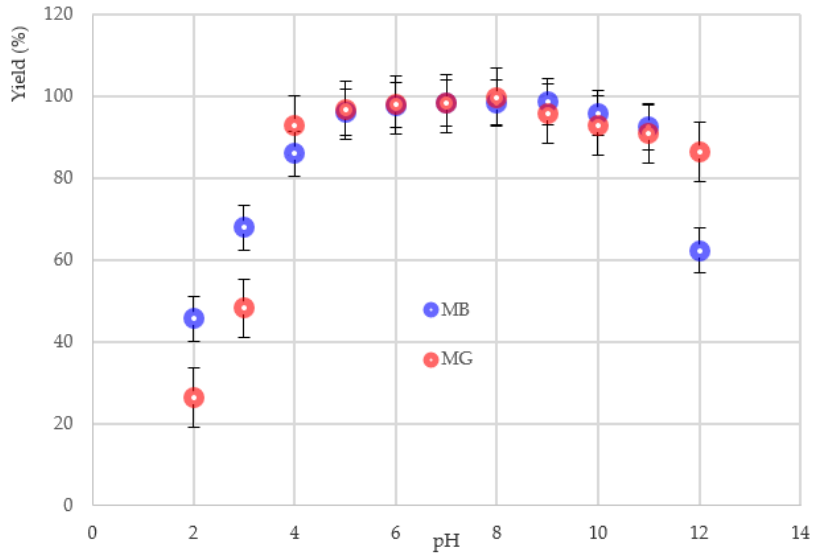

Figure 7. Effect of pH on the removal of MB and MG by 4AZW from aqueous solution. (C^0 (MB) = 11.5 mg/L, C^0 (MG) = 45 mg/L, S/L = 1 g/L, contact time 70 min, T = 25 ± 1 °C).

The highest adsorption capacities were obtained in the pH range of 5 to 10 for MB with a maximum adsorption efficiency of 99% at pH = 8.5. For MG, a relatively high adsorption capacity can be kept at pH = 5 to 11 with maximum adsorption of 99.5% at pH = 8 (Figure 7). Similar observations have also been reported by other researchers [48–53].

However, a definitive explanation of this point cannot be established on the basis of pH values only, because pH can be influenced, separately or together, by the surface charge of the adsorbent, the degree of ionization of the adsorbate, and the extent of dissociation of functional groups at the adsorbent active sites [44,54]. Lower sorption of dyes obtained at very acidic pH values can be explained through the behavior of the zeolite in acidic and basic mediums, as reported elsewhere [55].

First, zeolite in an acidic medium can easily exchange its M^+ metal cation with protons according to the following reaction:

$$[\text{Z-OM}]_n + H^+_{(aq)} \leftrightarrows [\text{Z-OH}]_n + M^+_{(aq)} \quad (4)$$

where Z is the Silicon or Aluminum atom at the solid surface and within the zeolite structure. This ion-exchange reaction leads to an increase in the solution pH as observed in Figure 7. If the initial H^+ concentration is high, proton adsorption at the neutral surface of the zeolite will take place:

$$[\text{Z-OH}]_n + H^+_{(aq)} \leftrightarrows [ZOH_2^+]_n \quad (5)$$

The protonation of the zeolite surface (Equation (5)) diminishes the possible dye adsorption due to electrostatic repulsive forces that may occur between the zeolite surface and the cationic dye. On the other hand, in an alkaline medium, hydroxyl ions can deprotonate the surface as follows:

$$[\text{Z-OH}]_n + OH^-_{(aq)} \leftrightarrows [ZO^-]_n + H_2O \quad (6)$$

Under such conditions, the attraction forces between the negatively charged zeolite surface and the positively charged MB and MG species favor the adsorption. Similar results have been obtained with other inorganic pollutants such as heavy metals in wastewater by using zeolite nanoparticles impregnated in polysulfone membranes [14].

3.6. Kinetics Studies

Kinetics models are important before any further investigation intothe mechanism of adsorption; the most popular are [56,57] the Lagergren's pseudo-first-order and the pseudo-second-order rate equations.

The pseudo-first-order equation is:

$$\frac{dq_t}{dt} = k_1.(q_e - q_t) \quad (7)$$

where q_t (mg/g) is the adsorption capacity at time t (min), k_1 is the rate constant of pseudo-first-order adsorption (min^{-1}), and qe (mg/g) is the equilibrium adsorption capacity. Integrating Equation (7) for boundary conditions (t = 0, q_t = 0 and t = t, q_t = q_t) leads to the nonlinear equation:

$$q_t = q_e.\left(1 - e^{-k_1.t}\right) \quad (8)$$

The rate equation for pseudo-second-order kinetics was given as [58]:

$$\frac{dq_t}{dt} = k_2.(q_e - q_t)^2 \quad (9)$$

Integrating Equation (9), using the boundary conditions at t = 0, q_t = 0 and with the amount of dye adsorbed being q_t for any time t, and after rearranging the corresponding rate law, one obtains:

$$q_t = \frac{k_2.q_e^2.t}{1 + k_2.q_e.t} \quad (10)$$

where k_2 (g/mg.min) is the pseudo-second-order rate constant.

The parameters obtained for the pseudo-second-order model are given in Table 2. At different dye concentrations, the pseudo-first-order model could not describe the entire range of adsorption time (detailed data not shown) and is limited only to the initial time range, as also described by others [57]. However, the pseudo-second-order data treatment presents higher determination coefficient (R^2) values and lower values for error analysis parameters. Furthermore, the corresponding $q_{e(cal)}$values are in better agreement with experimental data $q_{e(exp)}$. These results suggested that the pseudo-second-order model can be used to represent our adsorption data kinetics. For each dye, the k_2 value decreases when its concentration increases, and this might be related to higher competition for the adsorption sites when the dye concentration is high [59].

Table 2. Parameters for second-order kinetic model for removal of MB and MG dyes by 4AZW at 25 °C using nonlinearized model.

Parameters	MB				MG			
C_0 (mg/L)	5	15	20	25	10	20	35	50
$q_{e(exp)}$ (mg/g)	4.898	8.680	9.501	9.713	9.478	19.564	34.420	42.900
$q_{e(cal)}$ (mg/g)	4.903 ± 0.011	8.688 ± 0.091	9.560 ± 0.140	9.731 ± 0.117	9.503 ± 0.135	19.633 ± 0.153	34.480 ± 0.547	43.480 ± 0.646
k_2 (g/mg·min)	0.198 ± 0.009	0.054 ± 0.007	0.034 ± 0.002	0.030 ± 0.002	0.072 ± 0.022	0.054 ± 0.013	0.015 ± 0.004	0.007 ± 0.001
R^2	0.999	0.989	0.989	0.991	0.991	0.997	0.990	0.992
ARE (%)	0.10	0.09	0.62	0.18	0.26	0.35	0.17	1.35
SD	0.031	0.226	0.246	0.215	0.263	0.307	0.977	0.985

The relative error (ARE) function is a measure of the differences between the experimental amount of adsorbed dye and the value predicted by the model:

$$ARE(\%) = \frac{100}{n}\sum_{i=1}^{n}\frac{\left|q_{e(exp)} - q_{e(cal)}\right|}{q_{e(exp)}} \quad (11)$$

where n is the number of experiments (here n = 3). The values of ARE (%) for the second-order kinetic model are presented in Table 2.

3.7. Adsorption Isotherms

At higher initial dye concentrations, the mass transfer resistance between the solid surface and the solution can be more easily overcome. With an increasing concentration of dye, empty active centers at the adsorbent surface are rapidly filled. Thus, as the initial concentration increased, the adsorption capacity increased [60].

For the optimization of an adsorption process, it is important to establish the most appropriate correlation for the equilibrium curve. Two widely known isotherm models, namely the Langmuir and Freundlich models [56,61], were used in this study to describe the adsorption process of MB and MG onto 4AZW.

The Langmuir model assumes that only one solute species will occupy one active site on the homogeneous surface of the adsorbent, and the corresponding nonlinear equation is:

$$q_e = \frac{k_L.C_e.q_{max}}{1 + k_L.C_e} \quad (12)$$

where C_e is the equilibrium concentration of the adsorbate (mg/L), $C_0$is the initial concentration of the adsorbate (mg/L), and qmax (mg/g) and K_L(L/mg) are the maximum adsorption capacity and a constant related to the energy of adsorption, respectively. One can also introduce a separation factor:

$$R_L = \frac{1}{1 + k_L.C_0} \quad (13)$$

This is a useful dimensionless constant: The isotherm is either unfavorable (R_L> 1), linear (R_L = 1), favorable (0 < R_L < 1), or irreversible (R_L = 0) [56]. For the adsorption of MB and MG onto 4AZW, all the R_L values are in the range of 0.008 to 0.043 and 0.015 to 0.064, respectively. Then, the adsorption process is favorable.

The Freundlich isotherm is an empirical model assuming a process on heterogeneous adsorption surfaces, and is not restricted to monolayer formation. The corresponding nonlinear equation is:

$$q_e = k_F.C_e^{\frac{1}{n}} \quad (14)$$

where k_F (mg/g)/(mg/L)$^{1/n}$ and n (dimensionless) are constants representing the adsorption capacity and the adsorption intensity, respectively.

The Langmuir and Freundlich models were compared for our experimental results (Figure 8). On the basis of R_2 determination coefficients values, the Langmuir model gave high values for both dyes (0.993 and 0.994; see Table 3), while those obtained by the Freundlich model were lower (0.949 and 0.985, detailed data not shown). The Langmuir maximum adsorption capacity (q_{max}) for MB and MG onto 4AZW at 25 °C is determined as 9.95 mg/g (0.031 mmol/g) and 45.64 mg/g (0.125 mmol/g), respectively (Table 3).

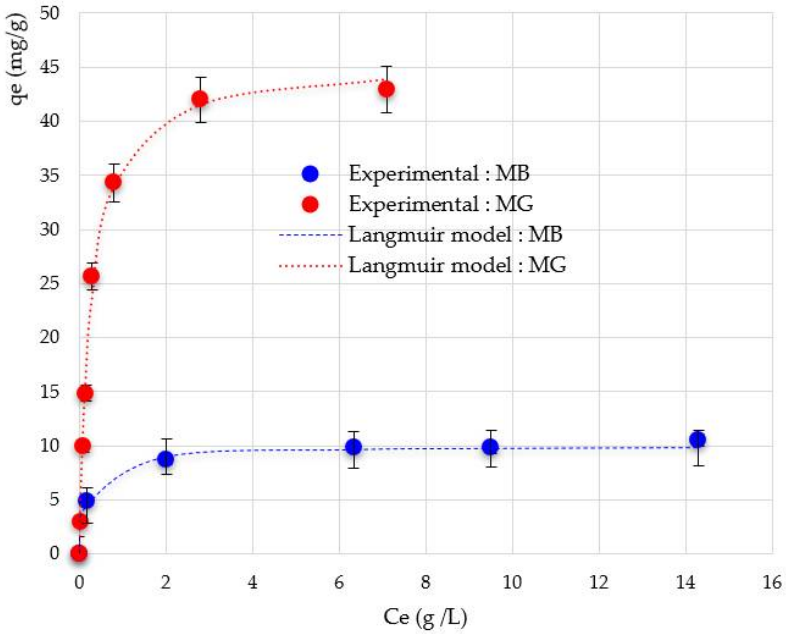

Figure 8. The Langmuir adsorption isotherms models for MB and MG adsorption on 4AZW(S/L = 1 g/L, T = 25 ± 1 °C and unadjusted pH), as a nonlinear expression.

Table 3. Parameters of Langmuir isotherm for removal of MB and MG onto 4AZW at 25 °C.

	MB				MG			
Langmuir	**q_{max} (mg/g)**	**K_L (L/mg)**	**R^2**	**SD**	**q_{max} (mg/g)**	**K_L (L/mg)**	**R^2**	**SD**
	9.95 ± 0.16	4.45 ± 0.54	0.993	0.241	45.64 ± 1.17	4.34 ± 0.20	0.994	0.315

3.8. Data Analysis by Response Surface Methodology

The optimization of the adsorption of MB on the 4AZW process needs 27 (that is: (3)3) experiences, but it can be reduced to 15 by using a BBD. The experimental design matrix and the predicted values obtained by BBD are compared to experimental data in Table 4, and the analysis of variance (ANOVA) allowed us to check the quality of the model (Table 5). The relationship between the experimental response (Yield (%)) and the uncoded forms of the three variables is:

$$Yield(\%) = 69.88 - 2.340X_1 + 1406X_2 - 6.50X_3 + 0.0395X_1^2 - 2605X_2^2 + 0.562X_3^2 - 33.64X_1.X_2 - 0.1523X_1.X_3 + 19.7X_2.X_3 \quad (15)$$

Table 4. The uncoded Box–Behnken design matrix of experiments for MB removal.

Run	Initial Dye Concentration (X_1) (mg/L)	Amount of Adsorbent (X_2) (g)	pH (X_3)	Yield (%)		
				Observed	Predicted	Residual
1	14	0.0250	4.0	42.46	43.00	−0.54125
2	8	0.0425	4.0	79.79	78.71	1.07375
3	8	0.0600	6.5	93.76	93.69	0.07000
4	8	0.0425	9.0	80.17	80.78	−0.61125
5	20	0.0425	4.0	40.05	39.44	0.61125
6	20	0.0250	6.5	20.34	20.41	−0.07000
7	14	0.0600	4.0	69.57	70.71	−1.14375
8	14	0.0425	6.5	53.15	52.89	0.25667
9	14	0.0250	9.0	39.92	38.77	1.14375
10	20	0.0425	9.0	31.29	32.36	−1.07375
11	14	0.0425	6.5	52.02	52.89	−0.87333
12	14	0.0425	6.5	53.51	52.89	0.61667
13	20	0.0600	6.5	43.31	42.77	0.53250
14	14	0.0600	9.0	70.47	69.93	0.54125
15	8	0.0250	6.5	56.66	57.19	−0.53250

Table 5. ANOVA for the fit of the experimental results to response surface model.

Factor	DF	Sum of Squares	Mean Square	*F*-Value	*p*-Value
Model	9	5719.41	635.49	395.15	<0.0001
X_1- Initial concentration	1	3845.21	3845.21	2390.96	<0.0001
X_2-m	1	1732.54	1732.54	1077.30	<0.0001
X_3-pH	1	12.55	12.55	7.80	0.038
X_1^2	1	7.47	7.47	4.64	0.084
X_2^2	1	2.35	2.35	1.46	0.281
X_3^2	1	45.48	45.48	28.28	0.003
$X_{1\times2}$	1	49.91	49.91	31.04	0.003
X_1X_3	1	20.88	20.88	12.99	0.015
X_2X_3	1	2.96	2.96	1.84	0.233
Residual	5	8.04	1.61		
Lack-of-fit	3	6.83	2.28	3.77	0.217
Pure Error	2	1.21	0.60		

Standard variation error S = 1.268; R^2 = 99.86%; $R^2_{adjusted}$ = 99.61%; $R^2_{predicted}$ = 98.04%.

The model Equation (15) indicates that the initial MB concentration (X_1) had a significant effect (p< 0.001, F = 2390) on the yield, followed by the amount of adsorbent m (X_2) and the solution pH (X_3) with a low F = 7.8. The positive coefficients of X_2, ($X_2.X_3$) and quadratic terms (X_{12}, X_{32}) indicated a direct effect on the removal yield of MB. In contrast, the negative terms X_1, X_3, ($X_1.X_2$), ($X_1.X_3$) and the quadratic term (X_{22}) had an inverse effect on MB adsorption. In addition, ANOVA results (Table 5) showed that this regression model was very significant with $p < 0.0001$ and F = 395.15. Moreover, regression analysis data indicated that quadratic terms X_{12}, X_{22}, and the interactive term $X_2.X_3$ are not significant at all ($p > 0.05$).

From Table 4, the agreement between the yield predicted by Equation (15) and the corresponding experimental data is very strong: The values of the determination coefficient R^2 = 0.9986 and of its adjusted R^2adj = 0.9961 indicate a good correlation between the observed and predicted values of MB removal efficiency. Finally, one can conclude that this experimental design is valid, because the error value is lesser than 5%.

Figure 9 illustrates the 3-D response surface plots of the removal efficiency of MB as a function of two independent variables: (a) The initial concentration C_0 and adsorbent dose m, (b) the initial concentration C_0 and pH, and (c) the adsorbent dose m and pH.

On the other hand, the optimum values of the variables X_1, X_2 and X_3 were obtained by solving the model Equation (15) with Minitab® 17, to establish the values of variables maximizing the removal yield. Figure 10 shows the optimization diagram obtained with the maximum desirability function (i.e., D = 1) for MB yield removal: In separate columns, the response is related to each of the three factors: Red vertical lines indicate the current factor settings, while the horizontal dotted lines show the response for the selected factor levels. In our case, the simulation was adjusted to maximize the adsorption percentage. The statistical sweet spot was determined for a maximal MB removal yield of 99.09% and a desirability of d = 1.0, leading to: C_0 = 8 mg/L, m = 0.06 g, and pH = 9.

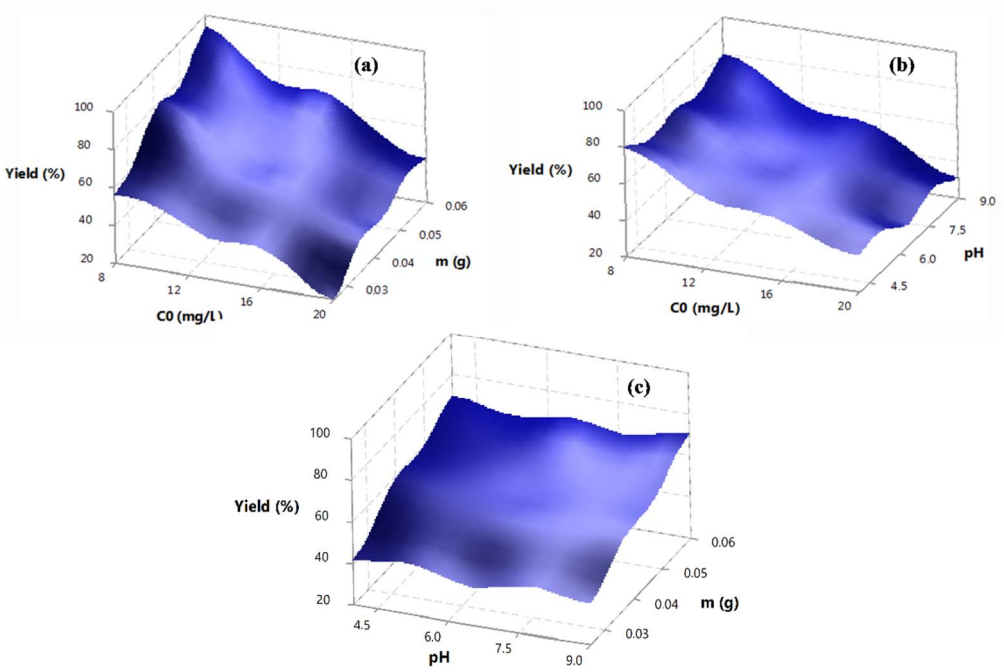

Figure 9. 3-D response surface plots for MB removal efficiency (%) onto 4AZW: (**a**) Effect of initial concentration/adsorbent dose; (**b**) effect of initial concentration/pH; (**c**) effect of adsorbent dose/pH.

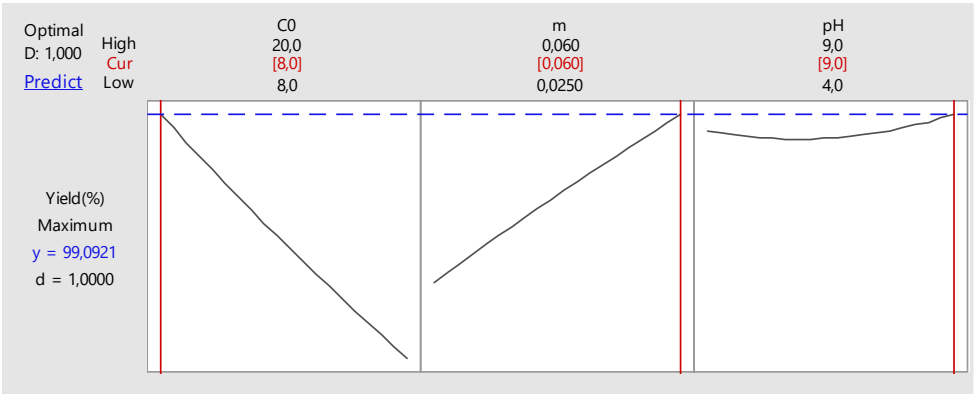

Figure 10. Diagrammatic optimization of MB removal parameters.

3.9. Thermodynamics Studies

To obtain complementary information on the feasibility of the process, standard thermodynamic parameters were calculated for the adsorption of either MB or MG on 4AZW at temperatures varying from 25 to 50 °C: The Gibbs free energy change (ΔG^0), enthalpy change (ΔH^0), and entropy change (ΔS^0).

The Gibbs free energy of adsorption ΔG^0 is derived from:

$$\Delta G^0 = -R.T.\ln\left(K_L^0\right) \quad (16)$$

where R= 8.314 J/mol.K is the universal gas constant, T is the absolute temperature (K), and $K_L{}^0$ is the (dimensionless) 'thermodynamic' Langmuir constant for the adsorption process. This value is calculated from K_L (L/mg) in the Langmuir model (Equation (12)), after changing all concentrations to molar form and considering the standard state C^0 = 1 mol/L [61–63]:

$$K_L^0 = K_L(L/mg)\ .1000\ (mg/g)\ .M\ (g/mol)\ .\ C^0\ (mol/L) \quad (17)$$

where M = 319.85 g/mol or M = 364.91 g/mol are the molar mass of MB or MG, respectively, and the factor 1000 converts g to mg.

The enthalpy (ΔH^0) and entropy (ΔS^0) parameters were estimated from the classical thermodynamic relationships:

$$K_L^0 = \exp\left(\frac{\Delta S^0}{R} - \frac{\Delta H^0}{R.T}\right) \quad (18)$$

$$\Delta G^0 = \Delta H^0 - T.\Delta S^0 \quad (19)$$

The non-linear plots (not shown) of the van′t Hoff Equation (18) allowed us to calculate ΔH^0 (kJ/mol) and ΔS^0 (J/mol.K). The values of ΔG^0 (kJ/mol) were again calculated from these values of ΔH^0 and ΔS^0 (see Table 6).

Table 6. Thermodynamic parameters for adsorption of MG and MB onto 4AZW.

Dye	T (K)	SD	K_L (L/mg)	$K_L{}^0$ ($\times 10^6$) (Dimensionless)	Ln $K_L{}^0$	ΔG^0 (kJ/mol)	ΔH^0 (kJ/mol)	ΔS^0 (J/mol.K)
MB	298	0.241	4.45 ± 0.54	1.42 ± 0.20	14.16 ± 0.14	−35.14 ± 0.37	18.68 ± 1.37	180.64 ± 4.09
	303	0.287	5.24 ± 0.68	1.67 ± 0.25	14.33 ± 0.15	−36.04 ± 0.40		
	313	0.338	6.71 ± 0.75	2.14 ± 0.28	14.57 ± 0.13	−37.85 ± 0.37		
	323	0.359	7.96 ± 0.70	2.54 ± 0.27	14.75 ± 0.11	−39.65 ± 0.31		
MG	298	0.315	4.34 ± 0.20	1.58 ± 0.10	14.27 ± 0.07	−35.41 ± 0.19	25.53 ± 1.12	204.53 ± 3.28
	303	0.214	5.47 ± 0.37	1.99 ± 0.17	14.50 ± 0.09	−36.43 ± 0.24		
	313	0.384	7.20 ± 0.28	2.62 ± 0.15	14.78 ± 0.06	−38.48 ± 0.18		
	323	0.299	9.84 ± 0.44	3.59 ± 0.23	15.09 ± 0.06	−40.52 ± 0.20		

The negative values of ΔG^0 slightly increase as temperature increases from 298 to 323 K; while they are negative at different temperatures, the adsorption process of MB and MG on 4AZW is favored and spontaneous. These values of ΔG^0 increased in the order 4AZW-MB < 4AZW-MG indicating that the adsorption was more spontaneous for the 4AZW-MG system than for the 4AZW-MB one [62].

Furthermore, both ΔH^0 values are positive, the characteristic of an endothermic process; for each dye, ΔH^0 < 40 kJ/mol, suggesting that their adsorption is a physically driven process [64]. With positive ΔS^0 for both dyes, there is an increase in the randomness of the system due to the desorption of water molecules from the adsorbent surface; similar results have also been reported by other research groups [51,65].

4. Conclusions

This study investigated the potential of 4AZWto remove two basic cationic dyes, MB and MG, from aqueous solutions under batch experimental conditions. It was observed that adsorption depends on the pH, adsorbent dose, contact time, and initial dye concentration. It is interesting to note that the initial solution pH is one of the key parameters in the MB and MG adsorption performance; the presence of salt in the solution decreased the adsorption by competitive inhibition.

According to kinetic data, the adsorption process could be defined by a pseudo-second-order kinetic model. The Langmuir model represented both systems (4AZW-MB and 4AZW-MG) giving maximum adsorption capacity (q_{max}) values of 9.95 mg/g and 45.64 mg/g, respectively, at 25 °C. A thermodynamic study revealed that the adsorption was spontaneous, endothermic, and physical in nature.

The analysis of our results performed by the Box–Behnken Design (BBD) for the adsorption of MB on 4AZW allowed us to define the corresponding optimum conditions: More than 99.09% MB removal with pH = 9; 4AZW load = 0.06 g in 50 mL; initial MB concentration = 8 mg/L and 70 min removal time at 25 °C.

Thus, the large amounts of 4A zeolite generated as solid waste by the natural gas dehydration units after several treatment cycles of the gas can be efficiently used as an adsorbent for these cationic dyes, without any specific treatment. Although it is well known

that zeolite is not a renewable natural resource, its use as an adsorbent has both practical and cost-effective advantages.

Author Contributions: Conceptualization, A.I., S.C. and L.M.; methodology, A.I., S.C., A.A. (Aymen Assadi) and L.M.; software, L.B. and A.T.; validation, J.-C.B., L.B., A.T., A.A. (Abdeltif Amrane), A.E.J. and L.M.; formal analysis, J.-C.B., L.B. and A.T.; investigation, A.I., A.A. (Aymen Assadi), L.B. and L.M.; resources, A.A. (Aymen Assadi) and L.M.; data curation, A.I., S.C.; writing—original draft preparation, A.I., S.C.; writing—review and editing, A.I., A.A. (Aymen Assadi), A.B., A.A. (Abdeltif Amrane) and L.M.; visualization, A.I., S.C., L.B. and J.-C.B.; supervision, J.-C.B., L.M. and A.A. (Aymen Assadi); project administration, L.M., A.A. (Aymen Assadi), A.E.J.; funding acquisition, A.E.J. All authors have read and agreed to the published version of the manuscript.

Funding: The authors extend their appreciation to the King Khalid University for funding this work through the Large Groups Project under grant number (R.G.P. 2/37/43).

Institutional Review Board Statement: Not applicable.

Informed Consent Statement: Not applicable.

Data Availability Statement: Not applicable.

Acknowledgments: This work was supported by King Khalid University, Abha, Saudi Arabia. The authors extend their appreciation to the Deanship of Scientific Research at King Khalid University for funding this work. The authors thank the University of Bouira (Algeria) for scientific collaboration.

Conflicts of Interest: The authors declare no conflict of interest.

References

1. Abada, Z.; Bouharkat, M. Study of management strategy of energy resources in Algeria. *Energy Rep.* **2018**, *4*, 1–7. [CrossRef]
2. Faramawy, S.; Zaki, T.; Sakr, A.A.E. Natural gas origin, composition, and processing: A review. *J. Nat. Gas. Sci. Eng.* **2016**, *34*, 34–54. [CrossRef]
3. Lenhard, L.G.; Andersen, S.M.; Coimbra-Araújo, C.H. Energy-environmental implications of shale gas exploration in Paraná hydrological basin, Brazil. *Renew. Sust. Energy Rev.* **2018**, *90*, 56–69. [CrossRef]
4. Santos, K.M.C.; Menezes, T.R.; Oliveira, M.R.; Silva, T.S.L.; Santos, K.S.; Barros, V.A.; Melo, D.C.; Ramos, A.L.; Santana, C.C.; Franceschi, E.; et al. Natural gas dehydration by adsorption using MOFs and silicas: A review. *Sep. Purif. Technol.* **2021**, *276*, 119409. [CrossRef]
5. Berg, F.; Pasel, C.; Eckardt, T.; Bathen, D. Temperature Swing Adsorption in natural gas processing: A concise overview. *ChemBioEng Rev.* **2019**, *6*, 59–71. [CrossRef]
6. Bahadori, A.; Vuthaluru, H.B. Simple methodology for sizing of absorbers for TEG (triethylene glycol) gas dehydration systems. *Energy* **2009**, *34*, 1910–1916. [CrossRef]
7. Santos, M.G.R.S.; Correia, L.M.S.; de Medeiros, J.L.; de Queiroz, O.; Araújo, F. Natural gas dehydration by molecular sieve in offshore plants: Impact of increasing carbon dioxide content. *Energy Convers. Manag.* **2017**, *149*, 760–773. [CrossRef]
8. Cundy, C.S.; Cox, P.A. The hydrothermal synthesis of zeolites: History and development from the earliest days to the present time. *Chem. Rev.* **2003**, *103*, 663–702. [CrossRef]
9. Englert, A.H.; Rubio, J. Characterization and environmental application of a Chilean natural zeolite. *Int. J. Min. Process.* **2005**, *75*, 21–29. [CrossRef]
10. Liu, H.; Zeng, S.; He, M.; He, P.; Jia, L.; Dong, F.; Yang, D.; Gao, J.; Wang, S.; Zhang, T.; et al. Remarkably enhanced activity of 4A zeolite modified Pt/reduced graphene oxide electrocatalyst towards methanol electrooxidation in alkaline medium. *Ionics* **2019**, *25*, 5131–5140. [CrossRef]
11. Khulbe, K.C.; Matsuura, T.; Feng, C.Y.; Ismail, A.F. Recent development on the effect of water/moisture on the performance of zeolite membrane and MMMs containing zeolite for gas separation; review. *RSC Adv.* **2016**, *6*, 42943–42961. [CrossRef]
12. Zito, P.F.; Brunetti, A.; Caravella, A.; Drioli, E.; Barbieri, G. Water vapor permeation and its influence on gases through a zeolite-4A membrane. *J. Membr. Sci.* **2019**, *574*, 154–163. [CrossRef]
13. Fertu, D.I.T.; Gavrilescu, M. Application of natural zeolites as sorbents in the clean-up of aqueous streams. *Environ. Eng. Manag. J.* **2012**, *11*, 867–878.
14. Yurekli, Y. Removal of heavy metals in wastewater by using zeolite nano-particles impregnated polysulfone membranes. *J. Hazard. Mater.* **2016**, *309*, 53–64. [CrossRef]
15. Ciosek, A.L.; Luk, G.K. Kinetic modelling of the removal of multiple heavy metallic ions from mine waste by natural zeolite sorption. *Water* **2017**, *9*, 482. [CrossRef]
16. Wang, S.; Peng, Y. Natural zeolites as effective adsorbents in water and wastewater treatment. *Chem. Eng. J.* **2010**, *156*, 11–24. [CrossRef]

17. Amin, M.T.; Alazba, A.A.; Manzoor, U. A review of removal of pollutants from water/wastewater using different types of nanomaterials. *Adv. Mater. Sci. Eng.* **2014**, *2014*, 825910. [CrossRef]
18. Mateen, F.; Javed, I.; Rafique, U.; Tabassum, N.; Sarfraz, M.; Safi, S.Z.; Yusoff, I.; Ashraf, M.A. New method for the adsorption of organic pollutants using natural zeolite incinerator ash (ZIA) and its application as an environmentally friendly and cost-effective adsorbent. *Desalination Water Treat.* **2016**, *57*, 6230–6238. [CrossRef]
19. Vítězová, M.; Jančiková, S.; Dordević, D.; Vítěz, T.; Elbl, J.; Hanišáková, N.; Jampílek, J.; Kushkevych, I. The possibility of using spent coffee grounds to improve wastewater treatment due to respiration activity of microorganisms. *Appl. Sci.* **2019**, *9*, 3155. [CrossRef]
20. Vyavahare, G.D.; Gurav, R.G.; Jadhav, P.P.; Patil, R.R.; Aware, C.B.; Jadhav, J.P. Response surface methodology optimization for sorption of malachite green dye on sugarcane bagasse biochar and evaluating the residual dye for phyto and cytogenotoxicity. *Chemosphere* **2018**, *194*, 306–315. [CrossRef] [PubMed]
21. Ahamad, T.; Naushad, M.; Eldesoky, G.E.; Al-Saeedi, S.I.; Nafady, A.; Al-Kadhi, N.S.; Al-Muhtaseb, A.H.; Khan, A.A.; Khan, A. Effective and fast adsorptive removal of toxic cationic dye (MB) from aqueous medium using amino-functionalized magnetic multiwall carbon nanotubes. *J. Mol. Liq.* **2019**, *282*, 154–161. [CrossRef]
22. Tanyol, M. Rapid malachite green removal from aqueous solution by natural zeolite: Process optimization by response surface methodology. *Desalination Water Treat.* **2017**, *65*, 294–303. [CrossRef]
23. Ani, J.U.; Okoro, U.C.; Aneke, L.E.; Onukwuli, O.D.; Obi, I.O.; Akpomie, K.G.; Ofomatah, A.C. Application of response surface methodology for optimization of dissolved solids adsorption by activated coal. *Appl. Water Sci.* **2019**, *9*, 60. [CrossRef]
24. Mirzabe, G.H.; Keshtkar, A.R. Application of response surface methodology for thorium adsorption on PVA/Fe_3O_4/SiO_2/APTES nanohybrid adsorbent. *J. Ind. Eng. Chem.* **2015**, *26*, 277–285. [CrossRef]
25. Varala, S.; Ravisankar, V.; Al-Ali, M.; Pownceby, M.I.; Parthasarathy, R.; Bhargava, S.K. Process optimization using response surface methodology for the removal of thorium from aqueous solutions using rice-husk. *Chemosphere* **2019**, *237*, 124488. [CrossRef]
26. Pansu, M.; Gautheyrou, J. *Handbook of Soil Analysis: Mineralogical, Organic and Inorganic Methods*; Springer: Berlin/Heidelberg, Germany; New York, NY, USA, 2006.
27. Primo Yúfera, E.; Carrasco Dorrien, J. *Química Agrícola*, 1st ed.; Alhambra: Madrid, Spain, 1973; Volume 1.
28. Kosmulski, M. *Surface Charging and Points of Zero Charge*; CRC Press: Boca Raton, FL, USA, 2009; ISBN 9781420051889.
29. Ferreira, S.L.C.; Bruns, R.E.; Ferreira, H.S.; Matos, G.D.; David, J.M.; Brandao, G.C.; da Silva, E.G.P.; Portugal, L.A.; Dos Reis, P.S.; Souza, A.S.; et al. Box-Behnken design: An alternative for the optimization of analytical methods. *Anal. Chim. Acta* **2007**, *597*, 179–186. [CrossRef]
30. Salahshoor, Z.; Shahbazi, A. Modeling and optimization of cationic dye adsorption onto modified SBA-15 by application of response surface methodology. *Desalination Water Treat.* **2016**, *57*, 13615–13631. [CrossRef]
31. Chowdhury, S.; Saha, P.D. Scale-up of a dye adsorption process using chemically modified rice husk: Optimization using response surface methodology. *Desalination Water Treat.* **2012**, *37*, 331–336. [CrossRef]
32. Mora, B.P.; Bellú, S.; Mangiameli, M.F.; Frascaroli, M.I.; González, J.C. Response surface methodology and optimization of arsenic continuous sorption process from contaminated water using chitosan. *J. Water Process. Eng.* **2019**, *32*, 100913. [CrossRef]
33. Treacy, M.M.J.; Higgins, J.B. *Collection of Simulated XRD Powder Patterns for Zeolites*, 4th ed.; Elsevier: Amsterdam, The Netherlands, 2001; ISBN 978-0-444-53067-7.
34. Ma, B.; Lothenbach, B. Synthesis, characterization, and thermodynamic study of selected Na-based zeolites. *Cem. Concr. Res.* **2020**, *135*, 106111. [CrossRef]
35. Mozgawa, W.; Król, M.; Barczyk, K. FT-IR studies of zeolites from different structural groups. *Chemik* **2011**, *65*, 667–674.
36. Feng, Y.; Dionysiou, D.D.; Wu, Y.; Zhou, H.; Xue, L.; He, S.; Yang, L. Adsorption of dyestuff from aqueous solutions through oxalic acid-modified swede rape straw: Adsorption process and disposal methodology of depleted bioadsorbents. *Bioresour. Technol.* **2013**, *138*, 191–197. [CrossRef] [PubMed]
37. Dallel, R.; Kesraoui, A.; Seffen, M. Biosorption of cationic dye onto "Phragmites australis" fibers: Characterization and mechanism. *J. Environ. Chem. Eng.* **2018**, *6*, 7247–7256. [CrossRef]
38. Parlayici, Ş. Alginate-coated perlite beads for the efficient removal of methylene blue, malachite green, and methyl violet from aqueous solutions: Kinetic, thermodynamic, and equilibrium studies. *J. Anal. Sci. Technol.* **2019**, *10*, 4. [CrossRef]
39. Kazemi, S.Y.; Biparva, P.; Ashtiani, E. *Cerastoderma lamarcki* shell as a natural, low cost and new adsorbent to removal of dye pollutant from aqueous solutions: Equilibrium and kinetic studies. *Ecol. Eng.* **2016**, *88*, 82–89. [CrossRef]
40. Alwared, A.I.; Jaeel, A.J.; Ismail, Z.Z. New application of eco-friendly biosorbent giant reed for removal of reactive dyes from water followed by sustainable path for recycling the dyes-loaded sludge in concrete mixes. *J. Mater. Cycles Waste Manag.* **2020**, *22*, 1036–1046. [CrossRef]
41. Fungaro, D.A.; Yamaura, M.; Carvalho, T.E.M.; Graciano, J.E.A. Zeolite from fly ash-iron oxide magnetic nanocomposite: Synthesis and application as an adsorbent for removal of contaminants from aqueous solution. In *Zeolites: Synthesis, Chemistry and Applications*; Andreyev, M.K., Zubkov, O.L., Eds.; Nova Science Publishers, Inc.: New York, NY, USA, 2012; pp. 1–34. ISBN 978-1-61942-861-4.
42. Zhang, Y.; Zhu, C.; Liu, F.; Yuan, Y.; Wu, H.; Li, A. Effects of ionic strength on removal of toxic pollutants from aqueous media with multifarious adsorbents: A review. *Sci. Total Environ.* **2019**, *646*, 265–279. [CrossRef]

43. Hu, Y.; Guo, T.; Ye, X.; Li, Q.; Guo, M.; Liu, H.; Wu, Z. Dye adsorption by resins: Effect of ionic strength on hydrophobic and electrostatic interactions. *Chem. Eng. J.* **2013**, *228*, 392–397. [CrossRef]
44. Stumm, W.; Kummert, R.; Sigg, L. A ligand exchange model for the adsorption of inorganic and organic ligands at hydrous oxide interfaces. *Croat. Chem. Acta* **1980**, *53*, 291–312.
45. Boukhemkhem, A.; Rida, K. Improvement adsorption capacity of methylene blue onto modified Tamazert kaolin. *Adsorpt. Sci. Technol.* **2017**, *35*, 753–773. [CrossRef]
46. Kishore, K.; Guha, S.N.; Mahadevan, J.; Moorthy, P.N.; Mittal, J.P. Redox reactions of methylene blue: A pulse radiolysis study. *Int. J. Radiat. Appl. Instr. Part. C Radiat. Phys. Chem.* **1989**, *34*, 721–727. [CrossRef]
47. Srivastava, S.; Sinha, R.; Roy, D. Toxicological effects of malachite green. *Aquat. Toxicol.* **2004**, *66*, 319–329. [CrossRef] [PubMed]
48. Gupta, V.K.; Mittal, A.; Krishnan, L.; Gajbe, V. Adsorption kinetics and column operations for the removal and recovery of malachite green from wastewater using bottom ash. *Sep. Purif. Technol.* **2004**, *40*, 87–96. [CrossRef]
49. Baran, E.; Acemioğlu, B. Competitive removal of malachite green and rhodamine B using clinoptilolite in a two-dye system. *Clays Clay Miner.* **2016**, *64*, 299–313. [CrossRef]
50. Han, R.; Wang, Y.; Zhao, X.; Wang, Y.; Xie, F.; Cheng, J.; Tang, M. Adsorption of methylene blue by phoenix tree leaf powder in a fixed-bed column: Experiments and prediction of breakthrough curves. *Desalination* **2009**, *245*, 284–297. [CrossRef]
51. Rida, K.; Bouraoui, S.; Hadnine, S. Adsorption of methylene blue from aqueous solution by kaolin and zeolite. *Appl. Clay Sci.* **2013**, *83–84*, 99–105. [CrossRef]
52. Tamez Uddin, M.D.; Akhtarul Islam, M.D.; Mahmud, S.; Rukanuzzaman, M.D. Adsorptive removal of methylene blue by tea waste. *J. Hazard. Mater.* **2009**, *164*, 53–60. [CrossRef] [PubMed]
53. Mouni, L.; Belkhiri, L.; Bollinger, J.C.; Bouzaza, A.; Assadi, A.; Tirri, A.; Dahmoune, F.; Madani, K.; Remini, H. Removal of Methylene Blue from aqueous solutions by adsorption on Kaolin: Kinetic and equilibrium studies. *Appl. Clay Sci.* **2018**, *153*, 38–45. [CrossRef]
54. Nandi, B.K.; Goswami, A.; Purkait, M.K. Removal of cationic dyes from aqueous solutions by kaolin: Kinetic and equilibrium studies. *Appl. Clay Sci.* **2009**, *42*, 583–590. [CrossRef]
55. Polatoglu, I.; Cakicioglu-Ozkan, F. Aqueous interactions of zeolitic material in acidic and basic solutions. *Microporous Mesoporous Mater.* **2010**, *132*, 219–225. [CrossRef]
56. Tran, H.N.; You, S.J.; Hosseini-Bandegharaei, A.; Chao, H.P. Mistakes and inconsistencies regarding adsorption of contaminants from aqueous solutions: A critical review. *Water Res.* **2017**, *120*, 88–116. [CrossRef]
57. Lima, E.C.; Sher, F.; Guleria, A.; Saeb, M.R.; Anastopoulos, I.; Tran, H.N.; Hosseini-Bandegharaei, A. Is one performing the treatment data of adsorption kinetics correctly? *J. Environ. Chem Eng.* **2021**, *9*, 104813. [CrossRef]
58. Ho, Y.S.; McKay, G. Pseudo-second order model for sorption processes. *Process. Biochem.* **1999**, *34*, 451–465. [CrossRef]
59. Chen, H.; Zhao, J.; Dai, G. Silkworm exuviae-A new non-conventional and low-cost adsorbent for removal of methylene blue from aqueous solutions. *J. Hazard. Mater.* **2011**, *186*, 1320–1327. [CrossRef] [PubMed]
60. Gobi, K.; Mashitah, M.D.; Vadivelu, V.M. Adsorptive removal of Methylene Blue using novel adsorbent from palm oil mill effluent waste activated sludge: Equilibrium, thermodynamics and kinetic studies. *Chem. Eng. J.* **2011**, *171*, 1246–1252. [CrossRef]
61. Tran, H.N.; Lima, E.C.; Juang, R.S.; Bollinger, J.C.; Chao, H.P. Thermodynamic parameters of liquid–phase adsorption process calculated from different equilibrium constants related to adsorption isotherms: A comparison study. *J. Environ. Chem. Eng.* **2021**, *9*, 106674. [CrossRef]
62. Salvestrini, S.; Leone, V.; Iovino, P.; Canzano, S.; Capasso, S. Considerations about the correct evaluation of sorption thermodynamic parameters from equilibrium isotherms. *J. Chem Thermodyn.* **2014**, *68*, 310–316. [CrossRef]
63. Zhou, X.; Zhou, X. The unit problem in the thermodynamic calculation of adsorption using the Langmuir equation. *Chem. Eng. Commun.* **2014**, *201*, 1459–1467. [CrossRef]
64. Raval, N.P.; Shah, P.U.; Shah, N.K. Malachite green "a cationic dye" and its removal from aqueous solution by adsorption. *Appl Water Sci.* **2017**, *7*, 3407–3445. [CrossRef]
65. Dahri, M.K.; Kooh, M.R.R.; Lim, L.B.L. Application of *Casuarina equisetifolia* needle for the removal of methylene blue and malachite green dyes from aqueous solution. *Alex. Eng. J.* **2015**, *54*, 1253–1263. [CrossRef]